Nonlinear atmospheric teleconnections

William W. Hsieh, Aiming Wu and Amir Shabbar

submitted to Bulletin of the American Meteorological Society

July, 2005

Affiliations:

Hsieh and Wu – Dept. of Earth and Ocean Sciences, University of British Columbia, Vancouver, BC, Canada

Shabbar – Meteorological Service of Canada, Toronto, Ontario, Canada

Corresponding Author:

William Hsieh, Dept. of Earth and Ocean Sciences, University of British Columbia, 6339 Stores Road, Vancouver, BC V6T 1Z4, Canada.

E-mail: whsieh@eos.ubc.ca

Abstract

Nonlinear atmospheric teleconnections, found to be related quadratically to the El Niño-Southern Oscillation and Arctic Oscillation indices, propagate perturbations into areas where classical linear teleconnections are insignificant.

Contemporaneous correlations between distant atmospheric variables, commonly referred to as teleconnections, reveal the propagation of perturbations over vast distances via the atmosphere. The El Niño-Southern Oscillation (ENSO) (McPhaden 2004; Neelin et al. 1998) in the tropical Pacific tends to excite the Pacific/North American (PNA) atmospheric teleconnection pattern (Horel and Wallace 1981; Wallace and Gutzler 1981) in the winter N. Hemisphere. Another N. Hemisphere winter teleconnection pattern which lies mainly over the Arctic and North Atlantic is the North Atlantic Oscillation (NAO), also referred to as the Arctic Oscillation (AO) (Thompson and Wallace 1998; Wallace and Gutzler 1981). The classical studies in teleconnections produced large standing wave patterns in the atmosphere for the PNA and AO. With the recent advance in nonlinear signal processing techniques, atmospheric teleconnections have turned out to be more complicated than classical linear teleconnections.

NONLINEAR PROJECTIONS. In recent years, the asymmetry between the warm and cold states of ENSO in the tropical Pacific, and the corresponding asymmetry in the extratropical winter teleconnection have been studied, mainly by composite methods (Hoerling et al. 1997; Lin and Derome 2004). Neural network (NN) models (Hsieh 2004; Hsieh and Tang 1998) offer potentially more powerful tools to extract nonlinear signals. In particular, linear

projection (LP) (Deser and Blackmon 1995) has been generalized to nonlinear projection (NLP) (Wu and Hsieh 2004a; Wu and Hsieh 2004b; Wu et al. 2005) using NN, where an ENSO or AO index x is nonlinearly projected to the winter extratropical N. Hemisphere climate anomaly variables $\mathbf{y}$. The least squares fit $\mathbf{y} = \mathbf{f}(x)$ is solved, with the nonlinear continuous mapping functions $\mathbf{f}$ given by the NN model.

Our previous studies have only examined the NLP applied to individual fields or separate geographic regions. In this paper, we interconnect 4 variables – sea level pressure (SLP), surface air temperature (SAT), 500 hPa geopotential height (Z500), and standardized precipitation (PRCP) – over the whole Northern Hemisphere. Furthermore we compare the atmospheric teleconnections from ENSO and from AO, examining the nonlinear connections between them. Most importantly, the traditional linear teleconnection patterns are strongly contrasted with the new nonlinear patterns.

Separate projections were made onto the winter N. Hemisphere SLP anomalies, SAT anomalies, Z500 anomalies, and PRCP anomalies from the ENSO and the AO index. See the Appendix for details of the methodology.

Videos for nonlinear projections. With $\mathbf{f}$ nonlinear, the $\mathbf{y}$ pattern associated with a fluctuating x is not given by a standing wave pattern, but changes continuously with x, and can only be viewed via videos (downloadable from http://www.ocgy.ubc.ca/~william/BAMS/), with Supplemental Video 1 showing the LP and NLP from the ENSO index onto the SLP, SAT, Z500 and PRCP anomalies, and Supplemental Video 2 projecting from the AO index. That NLP does not give a standing wave oscillation like the LP is evident in the videos.

Nonlinear projections of ENSO. The NLP solution can be decomposed into a linear and a nonlinear component. The linear component is simply LP, while the nonlinear component is NLP–LP. Applying principal component analysis (PCA) (Jolliffe 2002) to this nonlinear component yields a first mode containing over 99% of the variance (where the high percentage variance results from NLP–LP being a noiseless map from a single degree of freedom given by the ENSO or AO index). This PCA spatial pattern (i.e. the empirical orthogonal function, EOF) gives the nonlinear teleconnection pattern. In the NLP of the ENSO index onto Z500 anomalies, the linear component (Fig. 1a) gives the classic PNA teleconnection pattern, while the nonlinear teleconnection pattern (Fig. 1b) shows much stronger signals in the Europe-Atlantic sector than the linear teleconnection pattern (Fig. 1a). The PC time series (Fig. 1c) of the nonlinear component is essentially in quadratic response to the ENSO index (as can be verified easily by a polynomial fit). Thus the PC takes on large positive values whenever the ENSO index indicates a warm or a cold episode. The time-varying anomaly field from a PCA mode is the product of the EOF (Fig. 1b) and the corresponding PC time series (Fig. 1c), hence the pattern in Fig. 1b is excited during both warm and cold ENSO episodes. In particular, in the Europe-Atlantic sector, the presence of negative Z500 anomalies at high latitudes and positive anomalies at mid latitudes (Fig. 1b) means that the positive phase of the NAO is excited during both warm and cold ENSO episodes (as found by Wu and Hsieh 2004a).

Next, we examine the NLP of the ENSO index onto the SAT anomalies and the PRCP anomalies (Fig. 2). The NLP of the SLP anomalies and the Z500 anomalies are superimposed on the SAT and PRCP anomalies, respectively, so we can relate the SAT and PRCP anomalies to the circulation anomalies. In both Figs. 2a and b, the anomalies in the SAT are generally consistent with the interpretation that regions of positive and negative SLP anomalies have,

respectively, anomalous clockwise and anticlockwise circulation anomalies, and airflow from the south or the ocean raises the SAT while airflow from the north or from land lowers the SAT. For the SAT and PRCP anomalies, the PCs of their nonlinear components (Figs. 2c and d) are also quadratically related to the ENSO index, and because the quadratic relation is so dominant, the PCs in Figs. 2c, 2d and 1c are very similar to each other in appearance. The nonlinear teleconnection pattern of the PRCP anomalies (Fig. 2f) is generally consistent with the circulation patterns associated with the Z500 anomaly pattern (Fig. 2f), with airflow from the ocean or from the south raising the PRCP, and airflow from land or from the north lowering the PRCP. Most strikingly, while the linear teleconnection patterns of the 4 variables (Figs. 2a and e) are mainly concentrated in the North Pacific and western North America, the nonlinear teleconnection patterns (Figs. 2b and 2f) reveal strong signals in the Europe-North Atlantic-eastern North America region, consistent with the positive phase of the NAO being excited during both warm and cold ENSO episodes. Averaged over the N. Hemisphere (20ºN-90ºN), the variance contributed by the nonlinear component of the NLP for SLP, Z500, SAT and PRCP is, respectively, 34, 33, 30 and 42% that of the linear component.

Nonlinear projections of AO. The NLP of the AO index onto the winter N. Hemisphere SLP anomalies (Fig. 3) also reveals a nonlinear teleconnection pattern (Fig. 3b), though relative to the linear teleconnection pattern (Fig. 3a), it is not manifested as strongly as in the case of ENSO (Fig. 1). Again the PC of the nonlinear component reveals a basically quadratic relation with respect to the AO index (Fig. 3c). The linear AO teleconnection pattern is weak in the Pacific region relative to the Atlantic sector (Fig. 3a), in contrast, the nonlinear teleconnection pattern (Fig. 3b) displays its greatest strength in the N. Pacific.

The nonlinear teleconnection patterns for SAT (Fig. 4b) and PRCP (Fig. 4f) are again generally consistent with the circulation anomalies associated with the superimposed nonlinear teleconnection patterns of the SLP (Fig. 4b) and Z500 (Fig. 4f). While the linear teleconnection patterns for the AO (Figs. 4a and e) are focused on the Arctic-Atlantic-Europe region, the nonlinear patterns are relatively strong outside this region, manifesting strength in the N. Pacific and western N. America. Averaged over the N. Hemisphere, the variance of the nonlinear component of the NLP for SLP, Z500, SAT and PRCP is, respectively, 3, 3, 4 and 14% that of the linear component. While these averaged values are small, one must not forget that in specific regions and during specific times when the AO index has large amplitude, the nonlinear teleconnection effect can be stronger than the linear effect.

DISCUSSION AND SUMMARY. The strength of the nonlinear component is compared to the linear component in Fig. 5 for both the NLP of ENSO and AO. Clearly the nonlinear teleconnection of AO is much weaker than that of ENSO. Since the main region of ENSO activity is in the Pacific, while that of AO is in the N. Atlantic sector, it is remarkable that the nonlinear teleconnection effects from ENSO extend strongly into the N. Atlantic sector, and those from AO into the N. Pacific region. This suggests that the mechanism for nonlinear teleconnection allows farther propagation from the source region than that for linear teleconnection. The exact mechanism for nonlinear teleconnection is not clear; however, as anomalous winds $\mathbf{u}'$ and temperatures T' are expected to reverse sign as the ENSO or AO index reverses, the presence of quadratic terms like $\mathbf{u}'\bullet\nabla\mathbf{u}'$ and $\mathbf{u}'\bullet\nabla T'$ in the governing equations provides an explanation as to why the nonlinear response is mainly quadratic with respect to the ENSO or AO index. For extratropical seasonal climate predictions (Shabbar and Barnston

1996), incorporating nonlinear teleconnections may lead to enhanced forecast skills, with the red areas in Fig. 5 indicating regions where skill enhancements can be expected.

In summary, under nonlinear signal processing, atmospheric teleconnection has turned out to be more complicated than classical linear teleconnection, where a standing wave pattern oscillates according to how the ENSO or AO index changes. In addition to the linear component, there is now a nonlinear component oscillating according to the square of the ENSO or AO index. Thus regardless of whether the ENSO index swings positive or negative, this quadratic component excites the positive phase of the NAO in the Europe-Atlantic sector. Under nonlinear teleconnection, disturbances propagate further from the source region than under linear teleconnection, spreading the ENSO signal to the Europe-Atlantic sector, and the AO signal to the N. Pacific. Nonlinear teleconnections have been detected in the SAT and PRCP anomalies, as well as in the SLP and Z500 anomalies.

APPENDIX. The winter (November to March) data used were monthly data from 1948-2002, 20ºN-90ºN, with the 0.5º × 0.5º resolution land SAT and PRCP from the Climate Research Unit of the Univ. of East Anglia (http://www.cru.uea.ac.uk/~timm/grid/CRU_TS_2_0.html), the 5º × 5º resolution SLP from the National Center for Atmospheric Research (NCAR) (Trenberth and Paolino 1980), and the 2.5º × 2.5º Z500 from the National Centers for Environment Prediction (NCEP) reanalysis (Kalnay 1996). Anomalies were obtained by subtracting the climatological seasonal cycle. Only the leading 10 SLP, 10 Z500, 12 SAT and 13 PRCP principal components (PC) were retained, containing, respectively, 86, 81, 79 and 51% of the variance. The AO index is the standardized leading PC of the winter SLP anomalies, while the ENSO index is the leading PC of the winter

sea surface temperature (SST) anomalies over the tropical Pacific (20°S-20°N, 122°E-80°W) (using the 2º × 2º ERSST2 dataset from the National Climate Data Center, NOAA) (Smith and Reynolds 2004).

LP is simply linear regression with a single input (predictor) x (the ENSO or AO index) mapped to the output $\mathbf{y}$ (the leading PCs of the atmospheric anomalies), with no time lag, i.e. $\mathbf{y} = \tilde{\mathbf{c}}x + \mathbf{c}$, where $\tilde{\mathbf{c}}$ and $\mathbf{c}$ are regression coefficients. NLP is performed using a multi-layer perceptron NN model (Bishop 1995) with a single hidden layer (containing intermediate variables h_i, $i = 1, ..., m$), so the mapping is $x \rightarrow \mathbf{h} \rightarrow \mathbf{y}$, with

$$h_i = \tanh(w_i x + b_i), \quad y_j = \sum_i W_{ji} h_i + a_j,$$

where the model parameters $\mathbf{w}$, $\mathbf{b}$, $\mathbf{W}$ and $\mathbf{a}$ are determined by minimizing the mean square error (MSE) of $\mathbf{y}$. With large enough m, the NN is capable of modelling any nonlinear continuous function $\mathbf{y} = \mathbf{f}(x)$ to arbitrary accuracy (Bishop 1995). To avoid local minima during the optimization, the NN model was trained 30 times with random initial parameters, with the smallest MSE solution selected.

To reduce sampling dependence, we repeated the process 400 times, where each bootstrap (Efron and Tibshirani 1993) sample was obtained by randomly selecting (with replacement) one winter's data record 55 times from the original record of 55 winters. The ensemble mean of the resulting 400 NN models was used as the final model for the NLP. The final model was run with $m = 3$, after sensitivity tests showed the final model to be insensitive to m ranging from 2 to 5. The nonlinear teleconnection patterns in Figs. 1-4 are statistically significant at the 5% level, based on the bootstrap distributions.

REFERENCES

Bishop, C. M., 1995: Neural Networks for Pattern Recognition. Clarendon Pr., 482 pp.

Deser, C. and M. L. Blackmon, 1995: On the relationship between tropical and North Pacific sea surface temperature variations. J. Clim., 8, 1677-1680.

Efron, B. and R. J. Tibshirani, 1993: An Introduction to the Bootstrap. CRC Press, 436 pp.

Hoerling, M. P., A. Kumar, and M. Zhong, 1997: El Nino, La Nina and the nonlinearity of their teleconnections. J. Clim., 10, 1769-1786.

Horel, J. D. and J. M. Wallace, 1981: Planetary-scale atmospheric phenomena associated with the Southern Oscillation. Mon. Weath. Rev., 109, 813-829.

Hsieh, W. W., 2004: Nonlinear multivariate and time series analysis by neural network methods. Rev. Geophys., 42, RG1003, doi:10.1029/2002RG000112.

Hsieh, W. W. and B. Tang, 1998: Applying neural network models to prediction and data analysis in meteorology and oceanography. Bull. Am. Meteorol. Soc., 79, 1855-1870.

Jolliffe, I. T., 2002: Principal Component Analysis. Springer, 502 pp.

Kalnay, E. e. a., 1996: The NCEP/NCAR 40-year reanalysis project. Bull. Am. Meteorol. Soc., 77, 437-471.

Lin, H. and J. Derome, 2004: Nonlinearity of the extratropical response to tropical forcing. J. Clim., 17, 2597-2608.

McPhaden, M. J., 2004: Evolution of the 2002-03 El Niño. Bull. Am. Meteorol. Soc., 85, 677-695.

Neelin, J. D., D. S. Battisti, A. C. Hirst, F. F. Jin, Y. Wakata, T. Yamagata, and S. E. Zebiak, 1998: ENSO theory. J. Geophys. Res., 103, 14261-14290.

Shabbar, A. and A. G. Barnston, 1996: Skill of seasonal climate forecasts in Canada using Canonical Correlation Analysis. Mon. Weath. Rev., 124, 2370-2385.

Smith, T. M. and R. W. Reynolds, 2004: Improved extended reconstruction of SST (1854-1997). J. Clim., 17, 2466-2477.

Thompson, D. W. J. and J. M. Wallace, 1998: The Arctic Oscillation signature in the wintertime geopotential height and temperature fields. Geophys. Res. Lett., 25, 1297-1300.

Trenberth, K. E. and D. A. Paolino, Jr., 1980: The Northern Hemisphere sea-level pressure data set: trends, errors and discontinuities. Mon. Weath. Rev., 108, 855-872.

Wallace, J. M. and D. S. Gutzler, 1981: Teleconnections in the geopotential height fields during the northern hemisphere winter. Mon. Weath. Rev., 109, 784-812.

Wu, A. and W. W. Hsieh, 2004a: The nonlinear Northern Hemisphere atmospheric response to ENSO. Geophys. Res. Lett., 31, L02203, doi:10.1029/2003GL018885.

Wu, A. and W. W. Hsieh, 2004b: The nonlinear association between ENSO and the Euro-Atlantic winter sea level pressure. Clim. Dynam., 23, 859-868.

Wu, A., W. W. Hsieh, and A. Shabbar, 2005: The nonlinear patterns of North American winter temperature and precipitation associated with ENSO. J. Clim., 18, 1736-1752. DOI: 10.1175/JCLI3372.1.

FIGURE CAPTIONS.

Fig. 1 Spatial patterns for the (a) linear and (b) nonlinear components of the NLP model projecting from the ENSO index onto the winter Z500 anomalies (with no time lag). In (c), the PC associated with the EOF pattern in (b), and the ENSO index (dashed) are shown. Multiplying the pattern in (a) by the ENSO index yields the linear component, while multiplying the pattern in (b) by the PC in (c) yields the nonlinear component of the NLP. In (c), the PC is quadratically related to the ENSO index, (the PC is shown with zero mean due to the removal of the mean in the nonlinear component prior to performing the PCA).

Fig. 2 Spatial patterns for the (a) linear and (b) nonlinear components of the NLP model projecting from the ENSO index onto the winter SAT (°C) (colored) anomalies and the SLP (hPa) (contoured) anomalies, with the solid, dashed and thick contours representing positive, negative and zero values, respectively. In (c), the PC associated with the SAT pattern in (b), and the ENSO index (dashed) are shown. The PC for the SLP pattern in (b) would have largely overlapped with the PC of the SAT in (c), hence not shown. The linear and nonlinear patterns for PRCP (colored) and Z500 (m) (contoured) are shown in (e) and (f) respectively, and the PC for the nonlinear component of PRCP in (d).

Fig. 3 Spatial patterns for the (a) linear and (b) nonlinear components of the NLP model projecting from the AO index onto the winter SLP anomalies. In (c), the PC associated with the SLP EOF pattern in (b), and the AO index (dashed) are shown.

Fig. 4 Spatial patterns for the (a) linear and (b) nonlinear components of the NLP model projecting from the AO index onto the winter SAT (colored) anomalies and the SLP (contoured) anomalies. In (c), the PC of the SAT pattern in (b), and the AO index (dashed) are shown. The linear and nonlinear patterns for PRCP (colored) and Z500 (contoured) are shown in (e) and (f) respectively, and the PC for the nonlinear component of PRCP in (d).

Fig. 5 Plot of $\delta = (|\mathrm{NL}| - |\mathrm{L}|) / (|\mathrm{NL}| + |\mathrm{L}|)$, where NL and L are, respectively, the nonlinear and linear components of the NLP model for ENSO (top row) and for AO (bottom row), with δ for SAT given in (a) and (d), SLP in (b) and (e), and Z500 in (c) and (f). For PRCP, δ was rather noisy, hence not shown. Positive δ means the nonlinear component dominates over the linear component.

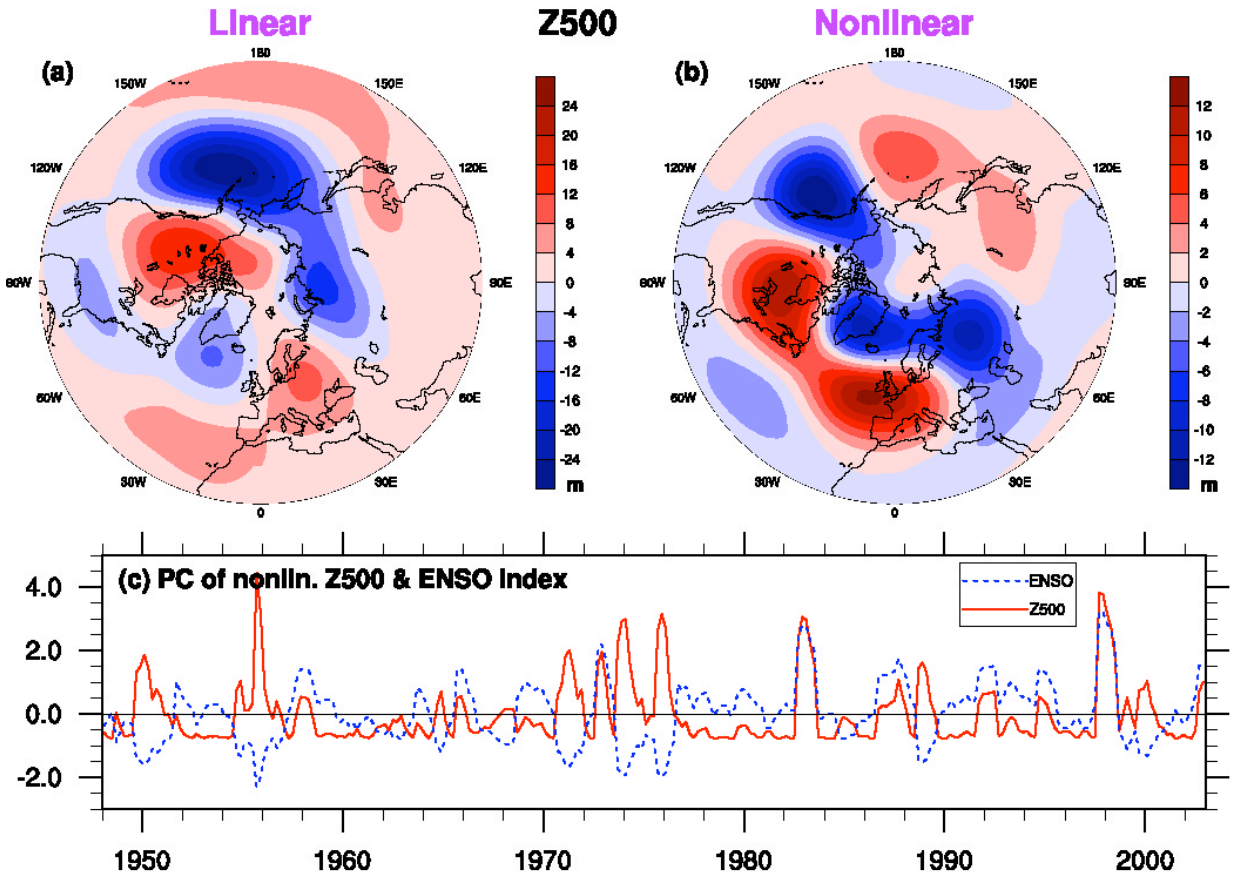

Fig. 1 Spatial patterns for the (a) linear and (b) nonlinear components of the NLP model projecting from the ENSO index onto the winter Z500 anomalies (with no time lag). In (c), the PC associated with the EOF pattern in (b), and the ENSO index (dashed) are shown. Multiplying the pattern in (a) by the ENSO index yields the linear component, while multiplying the pattern in (b) by the PC in (c) yields the nonlinear component of the NLP. In (c), the PC is quadratically related to the ENSO index, (the PC is shown with zero mean due to the removal of the mean in the nonlinear component prior to performing the PCA).

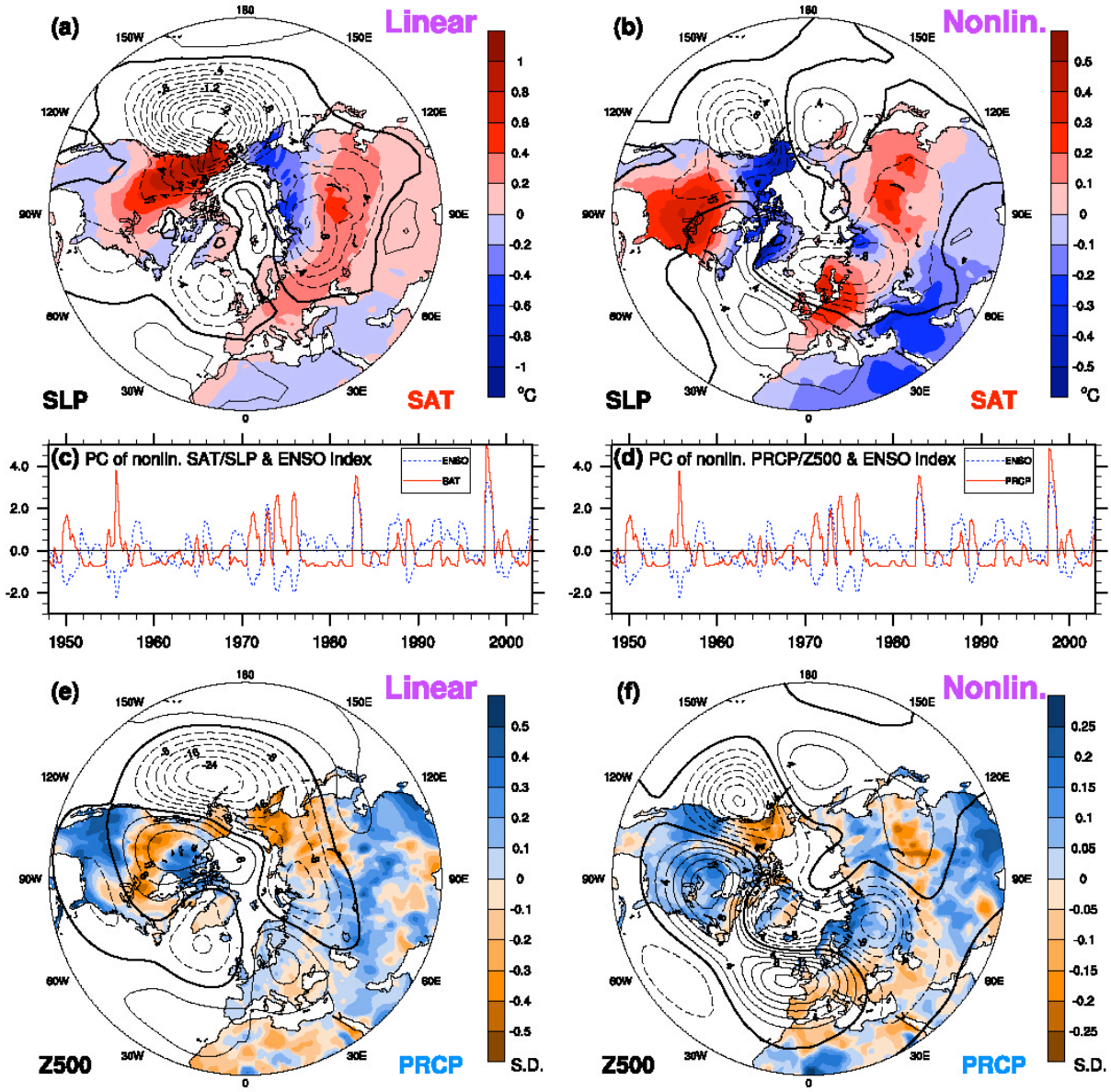

Fig. 2 Spatial patterns for the (a) linear and (b) nonlinear components of the NLP model projecting from the ENSO index onto the winter SAT (°C) (colored) anomalies and the SLP (hPa) (contoured) anomalies, with the solid, dashed and thick contours representing positive, negative and zero values, respectively. In (c), the PC associated with the SAT pattern in (b), and the ENSO index (dashed) are shown. The PC for the SLP pattern in (b) would have largely overlapped with the PC of the SAT in (c), hence not shown. The linear and nonlinear patterns for PRCP (colored) and Z500 (m) (contoured) are shown in (e) and (f) respectively, and the PC for the nonlinear component of PRCP in (d).

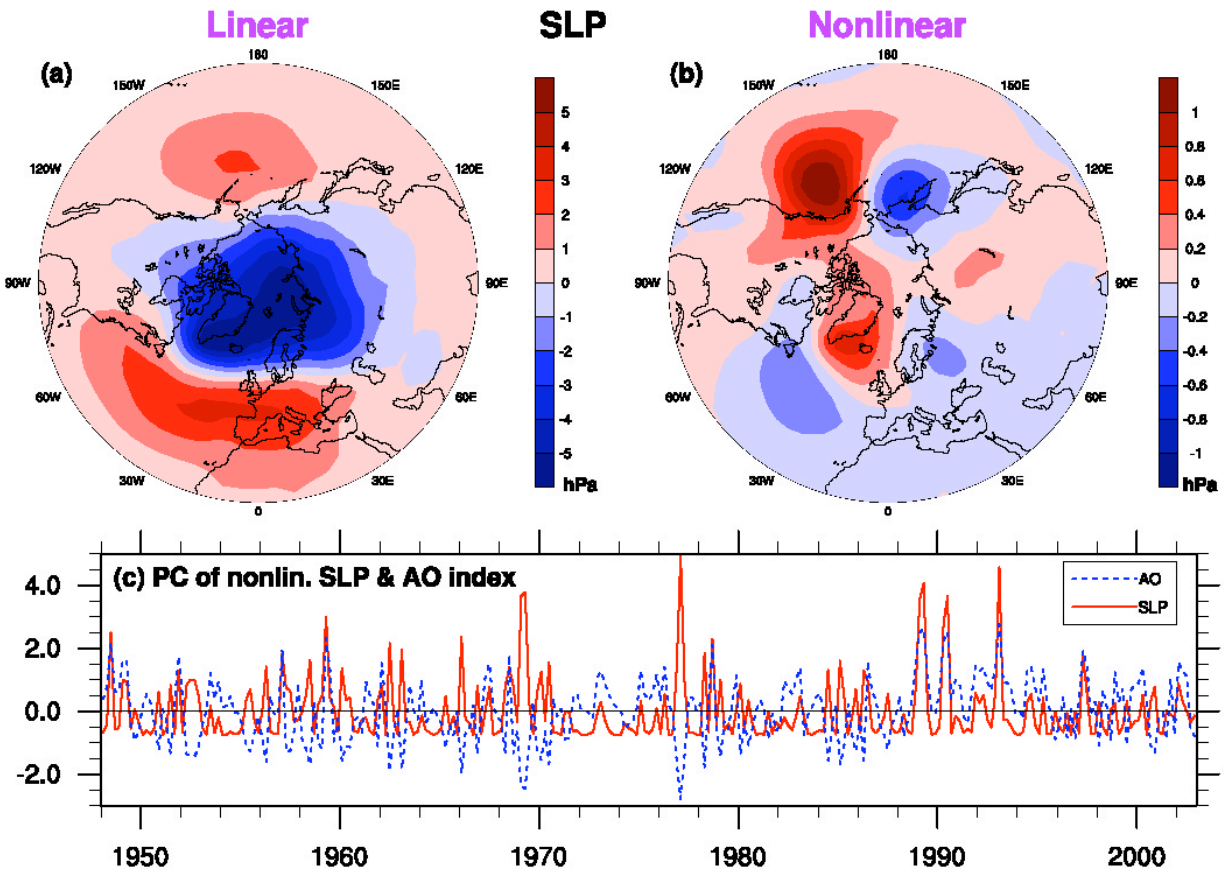

Fig. 3 Spatial patterns for the (a) linear and (b) nonlinear components of the NLP model projecting from the AO index onto the winter SLP anomalies. In (c), the PC associated with the SLP EOF pattern in (b), and the AO index (dashed) are shown.

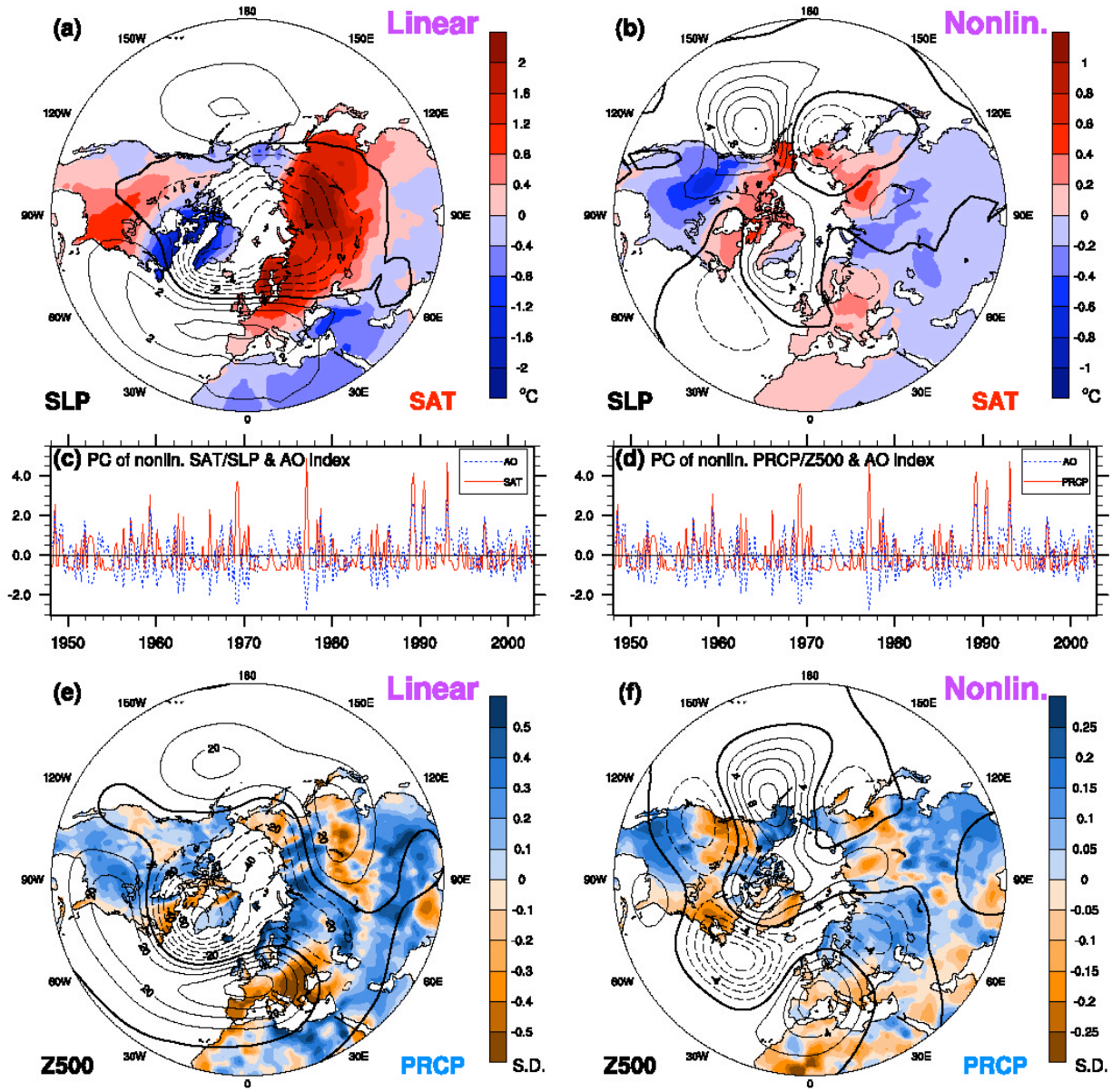

Fig. 4 Spatial patterns for the (a) linear and (b) nonlinear components of the NLP model projecting from the AO index onto the winter SAT (colored) anomalies and the SLP (contoured) anomalies. In (c), the PC of the SAT pattern in (b), and the AO index (dashed) are shown. The linear and nonlinear patterns for PRCP (colored) and Z500 (contoured) are shown in (e) and (f) respectively, and the PC for the nonlinear component of PRCP in (d).

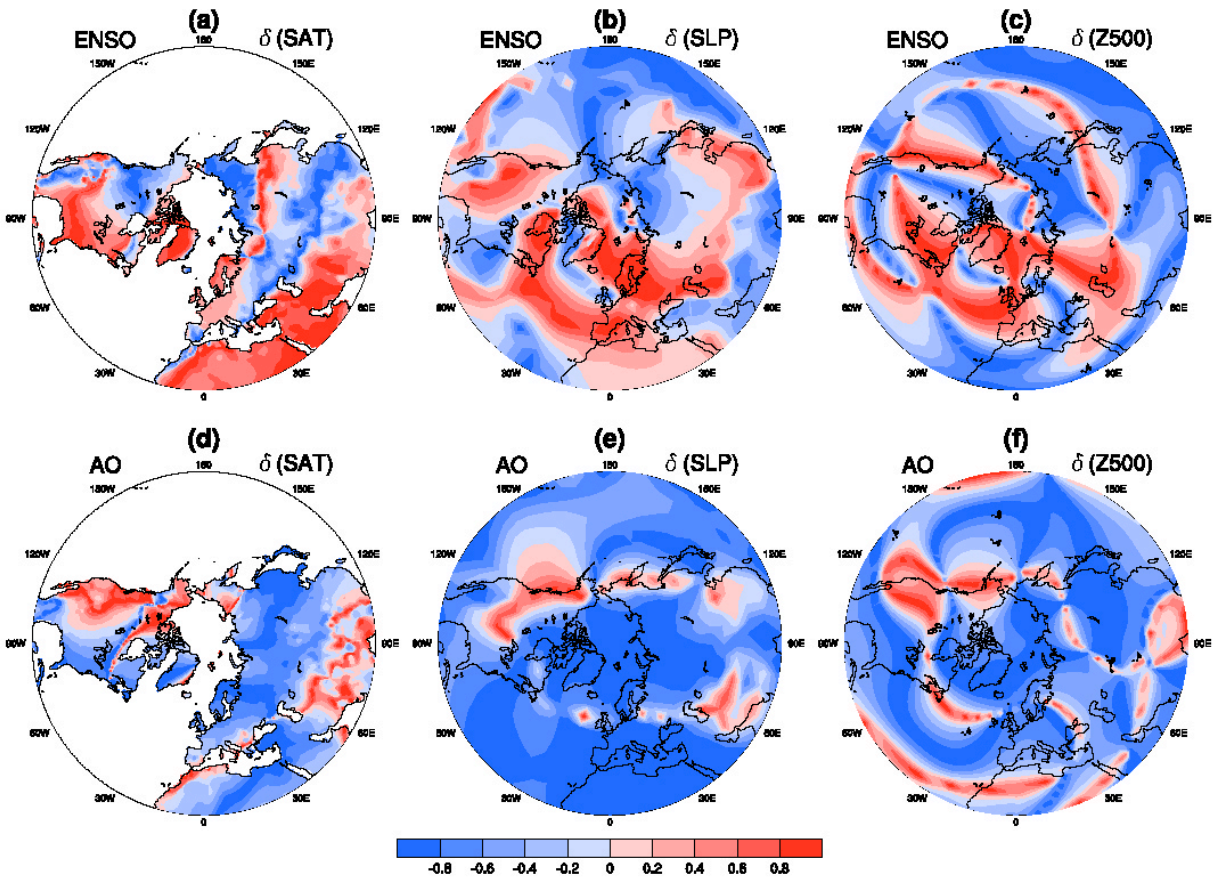

Fig. 5 Plot of $\delta = (|\mathrm{NL}| - |\mathrm{L}|) / (|\mathrm{NL}| + |\mathrm{L}|)$, where NL and L are, respectively, the nonlinear and linear components of the NLP model for ENSO (top row) and for AO (bottom row), with δ for SAT given in (a) and (d), SLP in (b) and (e), and Z500 in (c) and (f). For PRCP, δ was rather noisy, hence not shown. Positive δ means the nonlinear component dominates over the linear component.